Calculation of corrections to Fresnel optics from density response

K. Kempa and W. L. Schaich
Physics Department and Materials Research Institute, Indiana University, Bloomington, Indiana 47405
(Received 23 December 1985)

We develop a computational scheme for the Feibelman d parameters, which characterize the surface corrections to Fresnel formulas at a smooth jellium surface. The d parameters are determined from the nonretarded electronic density response to a long-wavelength field. We find this density response via the time-dependent Hartree approximation, which in turn requires the solution of a one-dimensional integral equation. The integral equation is analyzed in Fourier space, which allows us to isolate explicitly the nonanalytic structure in the kernel and to avoid the difficulties of long-ranged Friedel oscillations in the real-space kernel. The detailed formulas and procedures necessary to produce an efficient yet accurate computer code are described. As an initial illustration of the method, we calculate the linear dispersion coefficient of surface plasmons in a single, finite-step barrier model for the electrons. The results are compared to earlier calculations and to infinite barrier values. The evolution of the dispersion coefficient with barrier height shows interesting structure below the threshold for photoemission.

I. INTRODUCTION

In recent years there has been considerable theoretical work on the linear response of metal surfaces to electrodynamic fields. The analysis of a variety of experimental probes has led to an appreciation of what basic response functions contain the essential physics. This understanding is most clear for the response of jellium to externally incident, long-wavelength fields. Let us focus on this case and specifically examine the corrections to the Fresnel formulas for the reflection amplitude of such fields.

Consider a wave of frequency ω, incident at an angle θ_i on a smooth jellium surface. Define the following wave vectors: $Q=(\omega/c)\sin\theta_i$, for variations parallel to the surface, and $p_v=(\omega/c)\cos\theta_i$ and

$$p_m=[(\omega^2/c^2)\epsilon(\omega)-Q^2]^{1/2} ,$$

both for variations normal to the surface. One uses p_v outside and p_m inside the metal. In these equations c is the speed of light and $\epsilon(\omega)$ the (local) dielectric function of the bulk metal. For jellium

$$\epsilon(\omega)=1-\omega_B^2/\omega^2 , \tag{1}$$

with the bulk-plasma frequency ω_B determined by

$$\omega_B^2=\frac{4\pi n_B e^2}{m} , \tag{2}$$

where n_B is the bulk electronic density and $e<0$ and m the charge and mass of an electron. If the polarization of the wave lies in the plane of incidence (p wave), the Fresnel reflection amplitude is

$$r_p=\frac{\epsilon-p_m/p_v}{\epsilon+p_m/p_v} . \tag{3}$$

The result (3) follows from the well-known requirements of continuity of normal **D** field and parallel **E** field. However, this same theory also implies discontinuities in the parallel **D** and normal **E** fields, which cannot be true at the microscopic level. Indeed, the aim of recent theoretical work has been to develop a prescription for the calculation of the continuous variation of all field components through the surface region. Since several reviews of these derivations have already appeared,[1-4] we jump directly to their implications for the p-wave reflectivity. One finds in the limit of long (transverse) wavelengths that Eq. (3) must be replaced by

$$r_p=\frac{\epsilon-p_m/p_v-i(\epsilon-1)[(Q^2/p_v)d_\perp-p_m d_\parallel]}{\epsilon+p_m/p_v+i(\epsilon-1)[(Q^2/p_v)d_\perp+p_m d_\parallel]} \tag{4}$$

where the two (complex-valued) d parameters appear. Their unit is length, and d times wave vector gives the relative magnitude of the small corrections to both the numerator and denominator of the Fresnel formula.

It is useful to think of the d's as surface analogues of ϵ, in the sense that in the long-wavelength limit they all depend only on ω and serve to parametrize r_p. Like ϵ, the d's do not depend either on the angle of incidence or in any essential way[5] on the speed of light. For instance at fixed ω one can allow the incident wave to be decaying, i.e., to have $Q>\omega/c$ as physically occurs in an attenuated total reflection experiment or as may formally be imposed in the nonretarded description ($c\to\infty$) of fields due to charged probes. Still the same expression (4) holds for r_p with the same values of ϵ and d's.

This wide range of relevance means that the d's are important quantities in a host of surface phenomena.[1-3] Hence there is a strong theoretical motivation for their systematic calculation and several approaches have already been proposed. One may divide these into two basic schemes. The first, initiated by Feibelman,[6] works with the full set of Maxwell equations and determines the variations of all field components through the surface region. The key step in this approach is the solution of an integral

equation whose kernel is the current-current correlation function.[6–8] In effect, one simultaneously derives (4) and a prescription for the d's. For a p-wave field the results appear as

$$(1-\epsilon)d_{\parallel}=\int dx\frac{D_{\parallel}-D_{\parallel}^{0}}{E_{\parallel}^{0}} \tag{5}$$

$$(1-1/\epsilon)d_{\perp}=\int dx\frac{E_{\perp}-E_{\perp}^{0}}{D_{\perp}^{0}}\ , \tag{6}$$

where the integration is along the surface normal. The field components with no superscripts are the exact ones, while those with the zero superscript are the asymptotic form of their transverse parts far (tens of angstroms) from the surface. The latter are extrapolated into the surface region like (transverse) Fresnel fields and are discontinuous at the matching plane $x=0$. Hence, the integrands are significant only in the surface region, and the d's are readily calculated once the fields are known.

The second approach to the d's, stressed by Apell and coworkers,[1,3] is based on a further formal reduction of (5) and (6). For a flat surface with the edge of the constant, positive background charge density at $x=x_p$, one has

$$d_{\parallel}=x_p \tag{5'}$$

and if further $\omega<\omega_B$,[9]

$$d_{\perp}=\int dx\, x\,\delta\rho\Big/\int dx\,\delta\rho\ , \tag{6'}$$

where $\delta\rho$ is the charge density induced by a long-wavelength field at frequency ω. Since the d's do not depend on c,[5] one can formally let $c\to\infty$, and calculate $\delta\rho$ as a nonretarded response. Although this possibility is well known, it has generally not been exploited except for qualitative insight or formal constraints.[10,11] Only in the static limit[12,13] (or at imaginary frequencies[14]) have microscopic evaluations been done based on (6').

In this paper we present a procedure for calculating $d_{\perp}$ from nonretarded density response at arbitrary (real) frequencies. Our theory is an outgrowth of that by Gerhardts and Kempa,[8] but has been reformulated to emphasize density, rather than current, response. The basic formulas are derived in Sec. II and the Appendixes in Ref. 15. Then in Sec. III we present the results of model calculations of $d_{\perp}-d_{\parallel}$ at the $Q=0$, nonretarded surface plasmon frequency $\omega_B/\sqrt{2}$. These limited results allow a direct comparison with earlier estimates[16] of the surface-plasmon dispersion at low Q. More extensive calculations are in progress.

II. DERIVATION

Here we develop the equations used to calculate the induced density. Our present theory determines the density response within the time-dependent Hartree approximation [or random-phase approximation (RPA)] for otherwise free electrons near a smooth jellium surface. Since we want to elucidate the dependence of the response on the surface electronic structure, we need to vary the effective single-particle potential-energy barrier that confines the ground-state electrons to the metal. One may view these variations as due to an imposed, static, external potential,[17] although we shall only exhibit explicitly the total potential energy V each electron feels in the ground state, since that determines the basis orbitals. We assume that V depends only on the coordinate normal to the surface, $V=V(x)$, and that it quickly saturates away from the surface.

These basic approximations certainly have a quantitative significance, but will hopefully still allow qualitative insights. One knows how to remove most of them, at least piecewise. For instance, a reasonable allowance for the effects of exchange and correlation can be incorporated by using time-dependent local-density functional theory[18,19] instead of RPA. Such a theory has been applied at metal surfaces for the static response,[12,13,20,21] for the response at imaginary frequencies,[14] and for the response at real frequencies in systems of finite extent in at least one direction—spheres[22] or slabs.[23] Further, we shall note below, see Eq. (12), how this refinement can be included in our formalism. However, we feel that at present the extra calculational effort to include these effects is not warranted, given the other approximations we make. The model we examine has been simplified on purpose in order both to ease its evaluation and to aid its interpretation. Once its implications have been efficiently calculated and understood, then one can attempt to build more physics into it.

A. Basic integral equation

We need the electron density $\delta\rho(\mathbf{x},t)$ induced at first order by an external potential energy

$$V_e(\mathbf{x},t)=V_e(x;\underset{\sim}{Q},\omega)e^{i(\underset{\sim}{Q}\cdot\underset{\sim}{X}-\omega t)}\ .$$

All quantities will be at frequency ω and surface wave vector $\underset{\sim}{Q}$, so we omit henceforth the common factor $e^{i(\underset{\sim}{Q}\cdot\underset{\sim}{X}-\omega t)}$ and often write amplitudes without explicitly acknowledging their $\underset{\sim}{Q}$ and ω dependence; e.g.,

$$V_e(x;\underset{\sim}{Q},\omega)\to V_e(x)\ .$$

The perturbing potential is presumed to be of long wavelength. We locate the metal in $x>0$ and use

$$V_e(x;\underset{\sim}{Q},\omega)=\Gamma_e e^{-Qx}\ , \tag{7}$$

with Γ_e a constant, and eventually take the limit $Q=|\underset{\sim}{Q}|\to 0$.

The induced density at $\underset{\sim}{Q}$ and ω is formally determined by

$$\delta\rho(x;\underset{\sim}{Q},\omega)=\int dx'\chi(x,x';\underset{\sim}{Q},\omega)V_e(x';\underset{\sim}{Q},\omega)\ , \tag{8}$$

where χ is the full susceptibility. In the RPA, one reexpresses (8) as

$$\delta\rho(x;\underset{\sim}{Q},\omega)=\int dx'\chi_0(x,x';\underset{\sim}{Q},\omega)V_T(x';\underset{\sim}{Q},\omega)\ , \tag{9}$$

with

$$V_T(x;\underset{\sim}{Q},\omega)=V_e(x;\underset{\sim}{Q},\omega)+\int d\bar{x}\,V_c(x,x;\underset{\sim}{Q})\delta\rho(\bar{x};\underset{\sim}{Q},\omega)\ . \tag{10}$$

Here χ_0 is the independent-particle susceptibility, and V_T

is the total perturbing potential. The difference between V_T and V_e is due to the mean field of the induced density and in a dynamic Hartree theory that in turn is attributed to the direct Coulomb interaction

$$V_c(x,x';\underset{\sim}{Q})=\frac{2\pi e^2}{Q}e^{-Q|x-x'|} . \tag{11}$$

If one wished to include in the mean-field exchange and correlation effects within the local-density approximation, then V_c would be augmented by

$$V_{xc}(x,x';\underset{\sim}{Q},\omega)=\delta(x-x')\frac{d^2[n\varepsilon_{xc}(n)]}{dn^2}\bigg|_{n=n_0(x)} , \tag{12}$$

where $\varepsilon_{xc}(n)$ is the exchange-correlation energy per electron in a uniform electron gas of density n and $n_0(x)$ is the equilibrium density of electrons at location x.

Our method of solving (9) and (10) is based on Fourier cosine transforms defined as, e.g.,

$$V_e(q;\underset{\sim}{Q},\omega)=\int_0^\infty dx\cos(qx)V_e(x;\underset{\sim}{Q},\omega) \tag{13}$$

and

$$\chi_0(q,q';\underset{\sim}{Q},\omega)=\frac{2}{\pi}\int_0^\infty dx\cos(qx)\times\int_0^\infty dx'\cos(q'x')\times\chi_0(x,x';\underset{\sim}{Q},\omega) . \tag{14}$$

Here the origin for x is located outside the metal surface, so $n_0(x=0)$ is negligible. The choice of cosine transforms make the next several equations similar to those of Beck *et al.*,[24,25] although we stress that we need not assume that an infinite barrier exists at $x=0$. With the choice (7), one has

$$V_e(q)=\gamma_e v(q) , \tag{15}$$

where

$$\gamma_e=\frac{\Gamma_e Q}{4\pi e^2} \tag{16}$$

and

$$v(q)=\frac{4\pi e^2}{q^2+Q^2} , \tag{17}$$

the three-dimensional Fourier transform of the Coulomb potential energy. The same factor appears in the half-space transform of V_c:

$$V_c(q,q')=v(q)\delta(q-q')-\gamma v(q)v(q') , \tag{18}$$

with

$$\gamma=\frac{Q/\pi}{4\pi e^2} . \tag{19}$$

If we define $\delta\rho_0$ by

$$\delta\rho_0(x)=\int dx'\chi_0(x,x')V_e(x') , \tag{20}$$

then Eqs. (9) and (10) can be combined into

$$\begin{aligned}\delta\rho(q)&=\delta\rho_0(q)+\int_0^\infty d\bar{q}\int_0^\infty d\bar{q}'\chi_0(q,\bar{q})V_c(\bar{q},\bar{q}')\delta\rho(\bar{q}')\\&=\delta\rho_0(q)\left[1-\frac{\gamma}{\gamma_e}\int_0^\infty d\bar{q}\,v(\bar{q})\delta\rho(\bar{q})\right]\\&\quad+\int_0^\infty d\bar{q}\,\chi_0(q,\bar{q})v(\bar{q})\delta\rho(\bar{q}) .\end{aligned} \tag{21}$$

Next define

$$\lambda(\underset{\sim}{Q},\omega)=\frac{\gamma}{\gamma_e}\int_0^\infty dq\,v(q)\delta\rho(q) , \tag{22}$$

and write

$$\delta\rho(q)=\gamma_e(1-\lambda)[\nu(q)-1] . \tag{23}$$

Equation (21) then becomes

$$\nu(q)=1+\int_0^\infty dq'\chi_0(q,q')v(q')\nu(q') . \tag{24}$$

We describe the general evaluation of χ_0 in the next subsection, but here use one feature to reduce (24) some more. The cosine transform of the free-electron susceptibility χ_0 for a semi-infinite model has a diagonal piece whose strength is identical to the Fourier transform of χ_0 for a bulk system:

$$\chi_0(q,q')=\delta(q-q')\chi_{0,B}(q)+\bar{\chi}_0(q,q') . \tag{25}$$

Since the bulk dielectric function in RPA is

$$\epsilon_B(q;Q,\omega)=1-v(q)\chi_{0,B}(q) , \tag{26}$$

(24) becomes

$$\epsilon_B(q)\nu(q)=1+\int dq'\bar{\chi}_0(q,q')v(q')\nu(q') , \tag{27}$$

which is the basic integral equation we need to solve. In the limit of small or large q the relative contribution of the integral term becomes negligible so

$$\nu(q\to 0;Q\to 0,\omega)=1/\epsilon(\omega) , \tag{28}$$

with $\epsilon(\omega)$ defined in (1) while

$$\nu(q\to\infty)=1 . \tag{29}$$

If one ignores the integral term for all q, the theory is called the semiclassical infinite barrier model (SCIB). Although SCIB has been often used in surface response problems,[2,26,27] it suppresses precisely the dependences that we wish to study in that it allows no variation of the surface profile. Our theory is hence directed towards the efficient inclusion of the integral term in (27).

We complete this subsection by deriving the physical significance of the auxiliary functions introduced in Eqs. (22) and (23). First calculate the induced field outside the metal:

$$V_i(x;\underset{\sim}{Q},\omega)=\frac{2\pi e^2}{Q}\int_0^\infty dx'\,e^{-Q|x-x'|}\delta\rho(x';\underset{\sim}{Q},\omega) . \tag{30}$$

For $x<0$, one finds

$$V_i(x;\underset{\sim}{Q},\omega)=\Gamma_e\lambda(\underset{\sim}{Q},\omega)e^{Qx} . \tag{31}$$

Thus λ acts as an effective reflection amplitude of the externally applied potential (7). Indeed, $-\lambda$ is the nonretarded analogue of the r_p discussed in the Introduction. As $Q\to 0$, it becomes

$$-\lambda(Q=0,\omega)=\frac{\epsilon-1}{\epsilon+1}\ , \tag{32}$$

which follows from using (23) and (28) in (22) and agrees with (3). We do not go further to derive the analogue of (4), since this has already been done.[11]

Instead, we examine ν which determines $\delta\rho$ and in turn the d's and r_p. For $x>0$, one can ignore the -1 in (23) when calculating $\delta\rho(x)$:

$$\delta\rho(x>0)=\gamma_e(1-\lambda)\frac{2}{\pi}\int_0^\infty dq\,\nu(q)\cos(qx)\ . \tag{33}$$

Further, in the long-wavelength limit the prefactors in (33) may be reexpressed in terms of $D_\perp(0)$, the normal component of the net displacement field near the surface due to (7). Using Fresnel theory,

$$eD_\perp(0)=Q\Gamma_e\frac{2\epsilon}{1+\epsilon}=Q\Gamma_e(1-\lambda)\ . \tag{34}$$

Thus

$$4\pi e\,\delta\rho(x>0)=D_\perp(0)\frac{2}{\pi}\int_0^\infty dq\,\nu(q)\cos(qx)\ . \tag{35}$$

Again, in the long-wavelength limit, Poisson's equation is approximately

$$4\pi e\delta\rho(x)=\frac{\partial E_\perp(x)}{\partial x}\ , \tag{36}$$

which may be integrated using (35) to

$$E_\perp(x)-E_\perp(x_B)=D_\perp(0)\frac{2}{\pi}\int_0^\infty dq\,\frac{\nu(q)}{q}\times[\sin(qx)-\sin q(x_B)]\ , \tag{37}$$

where x_B ($>x>0$) is far into the metal. Formally allowing $x_B\to\infty$ yields

$$\frac{2}{\pi}\int_0^\infty dq\frac{\nu(q)}{q}\sin(qx_B)\to\nu(q\to0)=1/\epsilon\ , \tag{38}$$

but if we imagine that x_B is only far compared to the range of longitudinal fields (and $\delta\rho$) but short compared to the wavelength of transverse fields ($x_B\ll 1/Q$), then we can replace $E_\perp(x_B)\approx D_\perp(x_B)/\epsilon\approx D_\perp(0)/\epsilon$ so

$$E_\perp(x)=D_\perp(0)\frac{2}{\pi}\int_0^\infty dq\frac{\nu(q)}{q}\sin(qx) \tag{39}$$

or

$$E_\perp(x)=\frac{2}{\pi}\int dq\,D_\perp(q)\nu(q)\sin(qx)\ , \tag{40}$$

where $D_\perp(q)$ is the Fourier *sine* transform of the (nearly) constant normal displacement field. The interpretation of (40) is that $\nu(q)$ gives the ratio of Fourier sine transforms of E and D. Hence, what we call $\nu(q)$ is the same in the long-wavelength limit as the function $1/\bar{\epsilon}_l(\mathbf{q})$ of Gerhardts and Kempa.[8] The integral equation that they use to find their $1/\bar{\epsilon}_l(\mathbf{q})$ is equivalent to our (27) with a particular choice of $\bar{\chi}_0$ [see below Eq. (62)], but their derivation of this equation starts from a theory with full retardation and focuses on current response functions.

B. Independent-particle susceptibility

At zero surface wave vector the response kernel χ_0 in our model has the form

$$\chi_0(x,x')=\frac{2}{A}\sum_{\underset{\sim}{K}}\sum_k\sum_{k'}\frac{f_k-f_{k'}}{\epsilon_k+\hbar\omega-\epsilon_{k'}+i0^+}\times\psi_k(x)\psi_{k'}(x)\psi_{k'}(x')\psi_k(x')\ , \tag{41}$$

Here $\psi_k(x)$ is an eigenstate of electronic motion normal to the surface with eigenvalue $\epsilon_k=\hbar^2k^2/(2m)$. The motion parallel to the surface has already been separated off as a plane wave. When $\mathbf{Q}=\mathbf{0}$, the only reminders of this are the sum on parallel wave vector $\underset{\sim}{\mathbf{K}}$ scaled by one over the area A of the surface and the dependence of the zero temperature Fermi occupation factors on both k (or k') and $\underset{\sim}{\mathbf{K}}$:

$$f_k=\Theta\left[\epsilon_F-\epsilon_k-\frac{\hbar^2K^2}{2m}\right]\ , \tag{42}$$

where Θ is the unit step function and ϵ_F is the Fermi energy. The overall factor of 2 in (41) is for spin.

One of the normal wave-vector sums can be used to reexpress χ_0 as[2]

$$\chi_0(x,x')=\frac{2}{A}\sum_{\underset{\sim}{K}}\sum_k f_k\psi_k(x)\psi_k(x')\times[G(x,x';\epsilon_k+\hbar\omega)+G^*(x,x';\epsilon_k-\hbar\omega)]\ , \tag{43}$$

where

$$G(x,x';\epsilon)=\sum_{k'}\frac{\psi_{k'}(x)\psi_{k'}(x')}{\epsilon-\epsilon_{k'}+i0^+}\ , \tag{44}$$

and G^* is the complex conjugate of G. Since G is a one-dimensional, outgoing wave Green's function, we may alternatively write (44) as

$$G(x,x';\epsilon)=\psi^+(x_>)\psi^-(x_<)/W(\epsilon)\ , \tag{45}$$

where $\psi^+(x)$ and $\psi^-(x)$ are outgoing and incoming wave solutions, respectively, for motion normal to the surface at energy ϵ and $x_>$ ($x_<$) is the greater (lesser) of x and x'. The factor $W(\epsilon)$ is the Wronskian of these solutions and has the x independent value

$$W(\epsilon)=\frac{\hbar^2}{2m}\left[\frac{d\psi^+(x)}{dx}\psi^-(x)-\psi^+(x)\frac{d\psi^-(x)}{dx}\right]\ . \tag{46}$$

A qualitative sketch of $V(x)$ is drawn in Fig. 1. We assume that beyond $x=a>0$, $V(x)=0$, and that for x outside the metal, $V(x)\to V_B$. In the regions where $V(x)$ is constant, the $\psi^\pm(x)$ can be represented as either one or two partial waves. Their appearance is also sketched in Fig. 1. For $x>a$ the $\psi^\pm(x)$ may be explicitly written as

$$\psi^+(x>a)=e^{ik(x-a)} \tag{47}$$

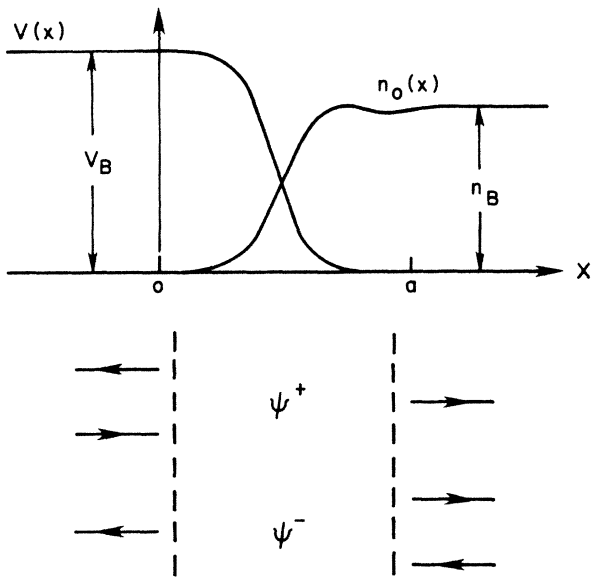

FIG. 1. Qualitative sketch of the surface potential-energy barrier and equilibrium density profile versus the coordinate normal to the surface. The asymptotic form of the one-electron states, $\psi^{\pm}$, is also indicated. The directions of the horizontal arrows indicate the propagation directions of the plane-wave components along the surface normal, in regions where V is constant. For $0<x<a$, $\psi^{\pm}$ are not so simply characterized.

$$\psi^-(x>a)=\sin[k(x-a)+\phi] , \tag{48}$$

so

$$W(\varepsilon)=-\frac{\hbar^2 k}{2m}e^{-i\phi} \tag{49}$$

and

$$G(x>a,x'>a;\varepsilon)=-(2m/\hbar^2 k)e^{ik(x_>-a)+i\phi} \times\sin[k(x_<-a)+\phi] . \tag{50}$$

In the above, k, which is $\sqrt{2m\varepsilon}/\hbar$, is chosen to be either positive real ($\varepsilon>0$) or positive imaginary ($\varepsilon<0$). The value of the phase shift ϕ depends on the shape of the potential barrier and on ε, but not on x or x'. For $\varepsilon>V_B$ or $\varepsilon<0$, ϕ is complex valued. The same phase shift also appears in the occupied states since for $0\leqq\varepsilon_k=\varepsilon\leqq\varepsilon_F$ one may set $\psi_k(x)\propto\psi^-(x)$.

Before writing out χ_0 again, we imagine changing to dimensionless quantities based on ratios to Fermi-level parameters; i.e., we divide wave vectors by k_F, multiply lengths by k_F, factor off k_F/ε_F from G, and divide frequencies by $\varepsilon_F/\hbar$. For simplicity we keep the same symbols for the dimensionless quantities. Then, using integrals instead of sums over wave vectors in (43), we can rewrite the integral equation (24) for $Q=0$ as

$$\nu(q)=1+\int_0^\infty dq' K(q,q')\nu(q') , \tag{51}$$

with

$$K(q,q')=K^{(l=1)}(q,q')+[K^{(l=-1)}(q,q')]^* , \tag{52}$$

where

$$K^{(l)}(q,q')=\frac{3\omega_B^2}{\pi}\int_0^1 dk(1-k^2)I^{(l)}(q,q',k)/(q')^2 . \tag{53}$$

The $I^{(l)}$ are defined by

$$I^{(l)}(q,q',k)=\int_0^\infty dx\cos(qx)\psi_k(x) \times\int_0^\infty dx'\cos(q'x')\psi_k(x') \times G(x,x';\varepsilon_k+l\omega) , \tag{54}$$

where ψ_k is normalized as in (48) and

$$\varepsilon_k+l\omega=(k_l)^2 , \tag{55}$$

with k_l either positive real or positive imaginary.

Compared to an analysis of the RPA integral equation in real space which must contend with long-ranged Friedel oscillations in $\chi_0(x,x')$ and $\delta\rho(x)$, our analysis in Fourier space offers the advantage of a short-ranged kernel $K(q,q')$. The information about Friedel oscillations now resides in nonanalytic behavior of K, or more specifically $I^{(l)}$, along a discrete set of loci in the (q,q') plane. The nonanalytic behavior usually arises from the large x and/or x' contributions to the integrals in (54) and can be extracted in closed form if necessary. To this end we separate (54) into bulk and surface parts

$$I^{(l)}=I_b^{(l)}+I_s^{(l)} , \tag{56}$$

where

$$I_b^{(l)}(q,q',k)=\int_a^\infty dx\cos(qx)\psi_k(x) \times\int_a^\infty dx'\cos(q'x')\psi_k(x') \times G(x,x';\varepsilon_k+l\omega) . \tag{57}$$

The restricted integration range for $I_b^{(l)}$ allows one to use (50) for G, and the resulting integrals can be done. However, their explicit derivation is complicated so we relegate them to Appendix A in Ref. 15 and present here only their final form.

Corresponding to (56) one can separate the K of (52) [or (53)] into K_b+K_s. We further write K_b as the sum of three pieces

$$K_b=\sum_{\lambda=1}^{3}K_{b,\lambda} . \tag{58}$$

The first contribution to (58) alone is nonzero if V is an infinite barrier at $x=a=0$. It contains the diagonal singularity responsible for (25)

$$K_{b,1}(q,q')=\delta(q-q')K_B(q)+\bar{K}_{b,1}(q,q') , \tag{59}$$

where, reverting momentarily to dimensioned quantities

$$K_B(q)=\chi_{0,B}(q)\frac{4\pi e^2}{q^2} , \tag{60}$$

with

$$\chi_{0,B}(q)=\frac{2}{(2\pi)^3}\int d^3k\frac{f_{\mathbf{k}}-f_{\mathbf{k}'}}{\varepsilon_k+\hbar\omega-\varepsilon_{k'}+i0^+}\ . \tag{61}$$

Here $k'=k\pm q$ and the integral runs over the whole of three-dimensional k space. This (bulk) Lindhard function is readily calculated.[8] The remaining function in (59) requires no integration over electronic states. It appears as

$$\frac{\pi(q')^2}{3\omega_B^2}K_{b,1}^{(l)}(q,q')=-\frac{\pi}{16}\sum_{\tau=\pm1}\frac{1}{l\omega+\tau qq'+i0^+}\{(1-k^2)\cos[2(\phi-ka)]\Theta(1-k)\}_{k=|(q+\tau q')/2|}\ . \tag{62}$$

In an unshifted infinite barrier model, one chooses $V=\infty$ for $x<a=0$. Then $\phi=0$ and the cosine function in (62) is unity; so our $\overline{K}_{b,1}(q,q')$ becomes identical to the function $-K(Q,Q')$ of Ref. 8. Hence, for such a model our integral equation for ν reduces to theirs.

The second contribution requires nontrivial integrals on k, which must be done numerically. These may be written as

$$\frac{\pi(q')^2}{3\omega_B^2}K_{b,2}^{(l)}(q,q')=\tfrac{1}{8}\int_0^1 dk(1-k^2)\sum_{\sigma,\tau,s}\frac{\sin(\phi+\sigma q^s a)}{\sigma q^s-\tau q^{-s}}N(k;\tau,-s,l)$$
$$\times\left[\mathrm{P}\frac{1}{l\omega+\sigma\tau qq'}\left[\mathrm{P}\frac{1}{k-\Delta^{\sigma\tau s}}-\mathrm{P}\frac{1}{k-\tau H^{l,-s}}\right]\right.$$
$$\left.+\frac{1}{l\omega+\sigma\tau qq'+i0^+}[-i\pi\tau\delta(k-\tau H^{l,-s})]\right]\ . \tag{63}$$

Here the P's denote principal-value integrals and the sums on σ, τ, and s all run over ±1. The new functions in (63) are defined by

$$q^s=\begin{cases}q, & s=1\\ q', & s=-1,\end{cases} \tag{64}$$

$$\Delta^{\sigma\tau s}=-\left[\frac{\sigma q^s+\tau q^{-s}}{2}\right], \tag{65}$$

$$H^{l,s}=\frac{l\omega-(q^s)^2}{2q^s}\ , \tag{66}$$

$$N(k;\sigma,s,l)=ik_l\sin(\phi+\sigma q^s a)-(k+\sigma q^s)\cos(\phi+\sigma q^s a)\ . \tag{67}$$

The argument of the sine function in (63) shows that in an infinite barrier model ($\phi=0$), $K_{b,2}$ will be nonzero only if a is nonzero.

The third contribution to (58) also requires numerical integrals on k. It appears as

$$\frac{\pi(q')^2}{3\omega_B^2}K_{b,3}^{(l)}(q,q')=-\tfrac{1}{8}\int_0^1 dk(1-k^2)\sum_{\sigma,\tau,s}\frac{e^{i\phi_l}\sin\phi_l}{k_l}\left[\frac{N(k;\sigma,s,l)}{l\omega+\sigma\tau qq'}\frac{N(k;\tau,-s,l)}{\sigma q^s-\tau q^{-s}}\left[\frac{P}{k-\tau H^{l,-s}}+i\pi\tau\delta(k-\tau H^{l,-s})\right]\right.$$
$$\left.+\frac{\pi^2}{q+q'}\frac{1-\sigma\tau}{2}(k^2+\omega)e^{-i(q+q')a}\delta(k-\tau H^{l,-s})\delta(l\omega-qq')\right]\ . \tag{68}$$

The only new function in (68) is ϕ_l the phase shift at the energy $\varepsilon_k+l\omega$. Since in an infinite barrier model $\phi_l=0$ for any a, $K_{b,3}$ is nonzero only for finite barriers.

In a similar fashion as for K_b, the results for K_s are conveniently split into a pair of contributions. Both require integrations on k and are simpler to write out than the $K_{b,\lambda}$ since fewer real-space integrals are done explicitly. From Appendix A in Ref. 15

$$K_s=K_{s,1}+K_{s,2}\ , \tag{69}$$

where

$$\frac{\pi(q')^2}{3\omega_B^2}K_{s,1}^{(l)}(q,q')=\tfrac{1}{4}\int_0^1 dk(1-k^2)\sum_{\tau,s}\frac{e^{i\phi_l}}{k_l}\frac{\tau}{q^{-s}}I^-(k;s,l)N(k;\tau,-s,l)\left[\frac{P}{k-\tau H^{l,-s}}+i\pi\tau\delta(k-\tau H^{l,-s})\right], \tag{70}$$

$$\frac{\pi(q')^2}{3\omega_B^2}K_{s,2}^{(l)}(q,q')=-\int_0^1 dk(1-k^2)\sum_s\frac{e^{i\phi_l}}{k_l}I^{-+}(k;s,l)\ . \tag{71}$$

The necessary real-space integrals are

$$I^{-}(k;s,l)=\int_0^a dx\,\cos(q^s x)\psi(x)\psi^{-}(x)\ , \tag{72}$$

$$I^{-+}(k;s,l)=\int_0^a dx\,\cos(q^s x)\psi(x)\psi^{-}(x) \times\int_0^a dx'\cos(q^{-s}x')\psi(x')\psi^{+}(x')\ . \tag{73}$$

Since these run over a bounded range, they have no δ function or principal value singularities like the $I_b^{(l)}$s.

To numerically determine K we need to integrate (63), (68), (70), and (71) over k. Where δ functions appear, the result is immediate; while the principal value integrals are generally done with the replacement

$$\int_0^1 dk\frac{g(k)}{k-k_0}=\int_0^1 dk\frac{g(k)-g(k_0)}{k-k_0}+g(k_0)\ln\left|\frac{1-k_0}{k_0}\right|\ , \tag{74}$$

where $g(k)$ is the nonsingular part of the integrand and k_0 is either $\tau H^{l,-s}$ or $\Delta^{\sigma\tau s}$. For the models we consider $g(k)$ is continuous, but its derivative can have isolated square-root singularities; e.g., the function k_l in (55) for $l=-1$ has such a divergent slope at $k=\omega$. To avoid difficulties due to these singularities we have found it sufficient to use their locations as endpoints in our Gaussian integration routines.

C. Solution of integral equation

Now turn to the numerical solution of (24), or its dimensionless form (51). The kernel K has various singularities which we separate out as follows:

$$K(q,q')=K_B(q)\delta(q-q')+K_H(q)\delta(qq'-\omega) +\frac{P}{qq'-\omega}K_h(q,q')+\hat{K}(q,q')\ . \tag{75}$$

Here K_B is the bulk Lindhard contribution defined in (60). Its inclusion converts (24) to (27). We refer to both of the next two terms as hyperbolic singularities since they are related to the hyperbola $qq'=\omega$. A physical argument for the appearance of these is given in Ref. 8. The δ function weight is shown in Appendix B in Ref. 15 to reduce to

$$\frac{\pi(q')^2}{3\omega_B^2}K_H(q)=i\frac{\pi^2}{16}e^{2i(\phi_+-k_+a)}[(1-k_-^2)\Theta(1-k_-) \times-(1-k_+^2)\Theta(1-k_+)]\ , \tag{76}$$

where $q'=\omega/q$ and

$$k_\pm=|q\pm q'|/2 \tag{77}$$

with $\phi_\pm=\phi(k_\pm)$. The strength of the principal-value singularity K_h, as well as the remainder term $\hat{K}$, require much more complicated formulas, which we leave in Appendix B in Ref. 15. The important point for the present discussion is that both contain no further singular values, although they do have discontinuous slopes across various curves in the (q,q') plane. However, just as in the calculation of K, we have found that using the locations of the troublesome nonanalytic points as the boundaries of separate q' integrals in (51) allows sufficient accuracy. The loci of nonanalyticity are described more in Appendix B in Ref. 15 and their appearance for a particular choice of ω and V_B are sketched in Fig. 5 in Ref. 15.

We solve (51) for $\omega<\omega_B$ by matrix inversion as in Ref. 8. The nontrivial integrations over q' are separated into the intervals $(0,\sqrt{\omega})$ and $(\sqrt{\omega},\infty)$. For the latter q' is replaced with $\tilde{q}'=\omega/q'$ so the integral over $\tilde{q}'$ also runs through the interval $(0,\sqrt{\omega})$. A discrete set of Gaussian integration points is then chosen to span the subintervals of smooth variation between $(0,\sqrt{\omega})$. Thus the numerical integration method makes q' discrete, and we impose the same mesh on q. To render the principal value integral numerically tractable, the same basic subtraction procedure as used in (74) is employed. Some refinements are needed since the singular point is included in the integration mesh—see Appendix B in Ref. 15. We have found it necessary when $\omega\approx\omega_B/\sqrt{2}$ to use a few hundred mesh points for the q' integrals, which in turn sets the size of the matrix inversion problem.

As a check on our numerical procedures, we have made various comparisons with the results of Ref. 8, whose code we started from. These calculations all represent the surface potential by an infinite barrier, but shift the location of the barrier away either from the origin, where the cosine tranforms start, or from a, where the potential reaches its constant bulk value of zero. These shifts have no physical consequence, but do require different mathematics in their solution because the shifting process can change various parts of the kernel K, in particular $K_{b,2}$ and K_s, from zero to nonzero values.

We show in Fig. 2 a comparison of the real part of the

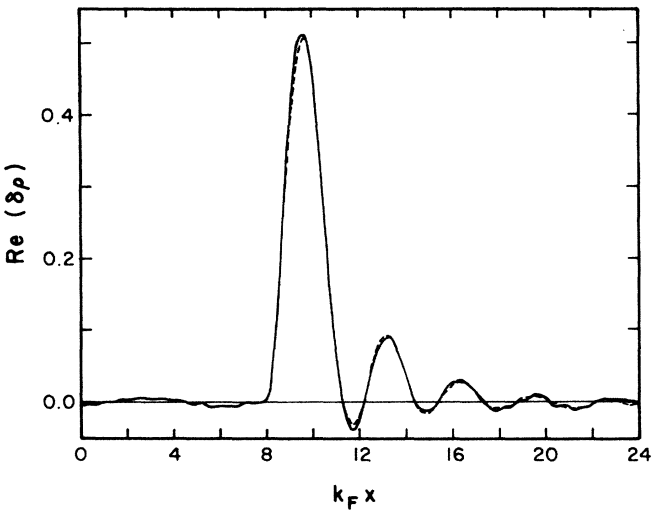

FIG. 2. Real part of the induced charge density in two mathematically distinct treatments of an infinite barrier model. In both cases $\int_{-\infty}^{\infty}k_F dx\,\delta\rho(x)=1$, $r_s=2.07$, and $\omega=\omega_B/\sqrt{2}$. The solid curve starts the cosine transforms at $x=0$, while the infinite barrier is at $k_F x=8$. The dashed curve in effect starts both the cosine transforms and the infinite barrier at $k_F x=8$ (Refs. 8 and 32); its $\delta\rho$ is identically zero for $k_F x<8$.

induced density of an infinite barrier model of Al evaluated in two such ways. Although there is more noticeable noise in the result for the shifted case, we consider the agreement satisfactory. The shifted calculation is done with $k_F a = 8$ and used 224 mesh points. Further increases in a alone make the errors larger because both the q and q' dependence of K are modulated by sinusoids of period of $2\pi/a$. Hence, an increase in a requires a proportional decrease in the integration mesh in order to keep the same accuracy.

III. INITIAL RESULTS

In this section we present some preliminary results for the case where the surface barrier is a single step of height V_B. The d's are evaluated once at the frequency $\omega_S = \omega_B/\sqrt{2}$ since that is sufficient to determine the dispersion relation of the long-wavelength surface plasmon via[28,29]

$$\omega(\underset{\sim}{Q}) = \omega_S[1 - \tfrac{1}{2}(d_\perp - d_{||})Q + \cdots] . \tag{78}$$

Of the two d's, $d_{||}$ is simpler to find since for our models it is a ground-state property and requires only the value of x_p, Eq. (5'). The latter can be determined from the Sugiyama sum rule,[30,31] which implies that if occupied states of normal motion vary for x deep within the metal as

$$\psi \rightarrow \sin[k(x - x_p) + \eta(k)] , \tag{79}$$

then

$$\pi/4 = \frac{2}{k_F^2} \int_0^{k_F} dK\, K \eta[(k_F^2 - K^2)^{1/2}] . \tag{80}$$

Comparing (79) with (48) yields

$$\eta(k) = \phi(k) + k(x_p - a) , \tag{81}$$

so we find after changing integration variables

$$k_F d_{||} = k_F x_p = \frac{3\pi}{8} - \frac{3}{k_F^2} \int_0^{k_f} dk\, k[\phi(k) - ka] . \tag{82}$$

For the occupied states behind a single-step barrier at $x = a$

$$\sin[\phi(k)] = \hbar k/(2mV_B)^{1/2} , \tag{83}$$

and the integral in (82) can be done analytically.

To find $d_\perp$ it is better not to use (6'), but instead to combine (6) and (39) into[8]

$$(1 - 1/\epsilon) d_\perp = \int_0^\infty dq \frac{1}{q^2}[v(q) - 1/\epsilon] . \tag{84}$$

This avoids the difficult numerical problem of accurately determining $\delta\rho$ for x far into the metal, where it is a slowly decaying sinusoid. The information on these Friedel oscillations is implicit in the nonanalytic structure of $v(q)$ at nonzero values of q, but is not very important for $d_\perp$. A more troublesome problem arises from the conflicting constraints that the origin be located far enough from the metal so all occupied states are negligible at $x = 0$, yet close enough to a where the potential saturates at its bulk value so the oscillation period of structure in $K(q,q')$ is minimized. It is necessary to reexamine this question for different systems since the optimal resolution depends on both barrier shape and bulk density.

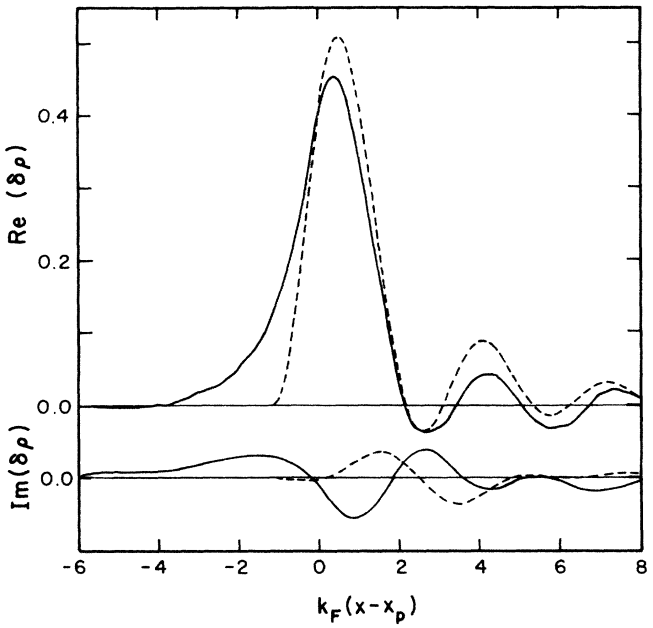

FIG. 3. Comparison of the induced charge density in finite (solid curves) and infinite (dashed curves) barrier models of Al. In both cases $\int_{-\infty}^{\infty} k_F dx\, \delta\rho(x) = 1$, $r_s = 2.07$, and $\omega = \omega_B/\sqrt{2}$. For the finite barrier, the work function is $\Phi = 4.16$ eV. The location of the jellium edge, x_p, is different for the two barriers. The infinite barrier starts at $k_F(x - x_p) = -3\pi/8$ while the finite-step barrier begins at $k_F(x - x_p) = -0.23$.

Even though we do not use $\delta\rho(x)$ directly to compute $d_\perp$, it is interesting to display it. Figure 3 shows both the real and imaginary parts of $\delta\rho$ at ω_S for a model that corresponds to Al. For the finite-step barrier results, we use 280 mesh points and set $k_F a = 8$; the infinite barrier curve is the same as the dashed curve in Fig. 2. Comparison with the shifted infinite barrier results of Fig. 2 shows that although the noise level is about the same, there are qualitative modifications in the distribution of the induced charge, which now extends further into vacuum. The imaginary part of $\delta\rho$ is especially changed, which in turn leads to a large enhancement of $-\mathrm{Im}(k_F d_\perp)$.

In Table I we list our results for the linear dispersion coefficient

$$A = \tfrac{1}{2} k_F (d_\perp - d_{||}) \tag{85}$$

for several nearly free electron metals and compare them to earlier calculations.[32–34] There is some ambiguity in parameter choices, since the free-electron values do not exactly match the experimental ones and because the surface barrier depends on which crystal face is exposed. We use free-electron quantities determined simply by the density parameter r_s and calculate V_B as $\varepsilon_F + \Phi$, where Φ is

the work function listed by Lang and Kohn[35] from data on polycrystals. By varying the number of mesh points, we believe that our numbers in the table are accurate to better than $\pm 5\%$. This convergence in A is possible with about half the number of mesh points used in Fig. 3.

The results attributed to Inglesfield and Wikborg have been extracted from a figure in their paper[33] and are consequently only quoted to one significant digit.[36] On this level, their answer is not inconsistent with ours, although the $\delta\rho$ they present in another paper[37] appears to have several qualitative differences with ours, most noticeably in its imaginary part. Since their number of mesh points is an order of magnitude less than that we use, perhaps their result for $\delta\rho$ is not fully converged. However, we cannot directly test this conjecture because their method of calculation is quite different from that used here. It works solely in real space and treats the integral equation (9) and (10) with $V_e=0$ as an eigenvalue equation.

A similar point of view is followed by Beck and Celli.[34] They differ from Inglesfield and Wikborg by introducing a variational method to analyze the eigenvalue equation. Their quoted result for the real part of A is quite different from ours, remaining always negative. It is interesting to note that their preferred variational form is (in our notation)

$$\delta\rho \propto e^{-\beta|x-\alpha|}\ , \tag{86}$$

with α chosen to be real. Using (86) in Eq. (6') implies $d_\perp=\alpha$. The α's that minimize the variational expression are always positive and larger than x_p. Indeed, Beck has informed us[36] that in the limit of zero surface wave vector that $\frac{1}{2}k_F(\alpha-x_p)$ is 0.16, 0.12, and 0.16, for Al, Mg, and Na, respectively. These values are considerably closer to our results in Table I, at least for the real part of A. However, the presumption of (86) with α real implies that $d_\perp$ is also real and, hence, that the imaginary part of A vanishes. It appears that we cannot simply reconcile the results of Beck and Celli with ours.

Finally, we compare the finite barrier results with those for an infinite barrier. They differ in some cases by more than an order of magnitude, and the changes do not develop smoothly in V_B. This is illustrated in Fig. 4 for several values of r_s. As one lowers V_B from infinity, both the real and imaginary parts of A decrease slowly in magnitude until $V_B \approx \varepsilon_F+\hbar\omega_S$, which is the threshold for photoemission. Further lowering of V_B leads to drastic changes. The real part of A, $\mathrm{Re}(A)$, goes through a minimum value which, depending on r_s, may be negative. However, for barrier heights matched to the calculations of Ref. 35, the single-step model predicts that $\mathrm{Re}(A)$ remains positive, but much smaller than its infinite barrier value. The imaginary part of A, $\mathrm{Im}(A)$, nearly vanishes close to the photoemission threshold. We cannot be more precise since values of $-\mathrm{Im}(A)$ below 10^{-3} can only be roughly estimated by our finite barrier code which has absolute errors of this magnitude.[38] The qualitative change in the imaginary part of $\delta\rho$ shown in Fig. 3 occurs as V_B passes through $\varepsilon_F+\hbar\omega_S$. The two profiles shown there then merge into each other not primarily by translations in x, but instead by both their amplitudes decreasing to zero. For further decreases of V_B, $-\mathrm{Im}(A)$ rises sharply and reverses its qualitative dependence on r_s. The change in $\mathrm{Im}(A)$ from its infinite barrier value is, hence, a sensitive function of the relative size of $\hbar\omega_S$ and Φ.

Figure 4 confirms the well-known sensitivity of the surface-plasmon dispersion relation to surface-electronic

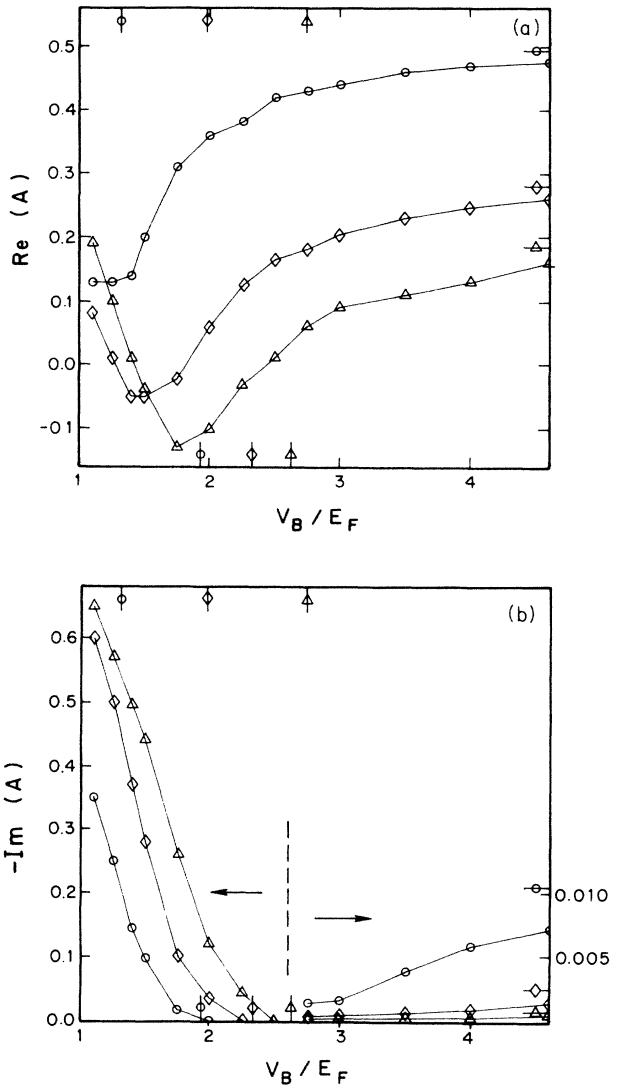

FIG. 4. (a) Real part of the surface plasmon, linear dispersion coefficient A versus single-step barrier height V_B. The calculations are denoted by circles for $r_s=2$, diamonds for $r_s=4$, and triangles for $r_s=6$. The lines connecting the points have only been drawn to guide the eye. The vertical bars at the top denote V_B values based on calculations in Ref. 35, while those at the bottom mark the threshold for photoemission: $V_B=\epsilon_F+\hbar\omega_S$. The horizontal bars on the right locate the infinite barrier results. (b) Imaginary part of the surface-plasmon linear dispersion coefficient A versus single-step barrier height V_B. The same labeling scheme is used as in (a). Note the change in vertical scale at $V_B/\varepsilon_F=2.6$.

TABLE I. Linear dispersion coefficient of the surface plasmon in a single-step barrier model.

Material	Refs.[a]	V_B/ε_F	ω_S/ω_F	$A=\frac{1}{2}k_F(d_\perp-d_{\parallel})$
Al ($r_s=2.07$)	KS	∞	0.96	$0.49-i0.0097$
	KS	1.36	0.96	$0.14-i0.17$
	IW	1.36	0.97	$0.2-i0.2$
	BC	1.36	0.86	$-0.12-i0.36$
	BC	1.36	0.86	$-0.24-i0.35$
Mg ($r_s=2.65$)	KS	∞	1.08	$0.40-i0.0066$
	KS	1.51	1.08	$0.085-i0.14$
	BC	1.51	1.08	$-0.23-i0.24$
	BC	1.51	1.08	$-0.22-i0.22$
Na ($r_s=3.99$)	KS	∞	1.33	$0.28-i0.0026$
	KS	1.86	1.33	$0.026-i0.078$
	BC	1.87	1.30	$-0.33-i0.24$

[a]References: IW is Ref. 33, BC is Ref. 34, and KS is the present work.

structure. It also implies that the unoccupied states play a significant role in this dependence. The rapid changes shown in Fig. 4 are puzzling if one attempts to correlate them only with the evolution of the equilibrium density profile, which gradually extends further out of the metal as V_B is lowered. The acknowledgment of an escape threshold for the unoccupied states seems to be a key point in the interpretation of the curves in Fig. 4. We are presently doing further calculations at different ω and for different barrier shapes in order to better understand the dependences of the d parameters. Since our numerical procedures can provide reasonably efficient and accurate evaluations of the d's, a systematic study is possible and we expect to report more results soon.

Note that the Appendixes and Fig. 5 have been deposited with the Physics Auxiliary Publication Service.[15]

ACKNOWLEDGMENTS

We are grateful both to Professor D. E. Beck for several useful discussions and for providing us with some unpublished results and to Professor R. R. Gerhardts for the suggestion to use density, instead of current, response functions as a basis for the calculations. This work was supported in part by the National Science Foundation (NSF) through grant No. DMR-81-15705, an especially important part of which was an addendum giving us access to the Cray-1 computer at Boeing Computer Services.

[1]P. Apell, Phys. Scr. **24**, 795 (1981).
[2]P. J. Feibelman, Prog. Surf. Sci. **12**, 287 (1982).
[3]P. Apell, Å. Lyungbert, and S. Lundqvist, Phys. Scr. **30**, 367 (1984).
[4]K. Kempa and R. R. Gerhardts, Surf. Sci. **150**, 157 (1985).
[5]The d's depend on c if relativistic effects are included in the electron dynamics, e.g., spin-orbit coupling. We ignore such dependencies here.
[6]P. J. Feibelman, Phys. Rev. B **12**, 1319 (1975).
[7]T. Maniv and H. Metiu, Phys. Rev. B **22**, 4731 (1980); J. Chem. Phys. **76**, 2697 (1982).
[8]R. R. Gerhardts and K. Kempa, Phys. Rev. B **30**, 5704 (1984).
[9]For $\omega>\omega_B$, a slightly more complicated result is necessary; see Ref. 2.
[10]B. N. J. Persson and P. Apell, Phys. Rev. B **27**, 6058 (1983).
[11]B. N. J. Persson and E. Zaremba, Phys. Rev. B **30**, 5569 (1984).
[12]N. D. Lang and W. Kohn, Phys. Rev. B **7**, 3541 (1973); N. D. Lang, in *Solid State Physics,* edited by H. Ehrenreich, F. Seitz, and D. Turnbull (Academic, New York, 1973), Vol. 28, p. 225.
[13]A. Liebsch, Phys. Rev. Lett. **54**, 67 (1985); Phys. Rev. B **32**, 6255 (1985).
[14]A. Liebsch, Phys. Rev. B **33**, 7249 (1986).
[15]See AIP document no. PAPS PRBMDO-34-547-16 for 16 pages containing Appendixs A and B as well as Fig. 5. Order by PAPS number and journal reference from American Institute of Physics, Physics Auxiliary Publication Service, 335 East 45th Street, New York, NY 10017. The prepaid price is $1.50 for a microfiche, or $5.00 for a photocopy. Airmail additional. Make checks payable to the American Institute of Physics.
[16]D. E. Beck and B. B. Dasgupta, in *Electromagnetic Surface Modes,* edited by A. D. Boardman (Wiley, London, 1982).
[17]M. Rasolt and F. Perrot, Phys. Rev. B **28**, 6749 (1983).
[18]A. Zangwill and P. Soven, Phys. Rev. A **21**, 1561 (1980).
[19]M. J. Stott and E. Zaremba, Phys. Rev. A **21**, 12 (1980).
[20]J. F. Dobson and J. H. Rose, J. Phys. C **15**, 7429 (1982).
[21]A. G. Eguiluz, Phys. Rev. B **31**, 3303 (1985).
[22]W. Ekardt, Phys. Rev. Lett. **52**, 1925 (1984).
[23]A. G. Eguiluz and D. A. Campbell, Phys. Rev. B **31**, 7572 (1985).
[24]D. E. Beck, V. Celli, G. LoVecchio, and A. Magnaterra, Nuovo Cimento B **68**, 230 (1970).
[25]D. E. Beck and V. Celli, Phys. Rev. B **2**, 2955 (1970).
[26]G. W. Ford and W. H. Weber, Phys. Rep. **113**, 195 (1984).
[27]F. Garcia-Moliner and F. Flores, *Introduction to the Theory of Solid Surfaces* (Cambridge University Press, New York, 1979).
[28]J. Harris and A. Griffin, Phys. Lett. **349**, 51 (1971).
[29]F. Flores and F. Garcia-Moliner, Solid State Commun. **11**, 1295 (1972).

[30]A. Sugiyama, J. Phys. Soc. Jpn. **15**, 965 (1960).
[31]D. C. Langreth, Phys. Rev. B **5**, 2842 (1972).
[32]K. Kempa and W. L. Schaich, Phys. Rev. B **32**, 8375 (1985).
[33]J. E. Inglesfield and E. Wikborg, J. Phys. C **6**, L158 (1973).
[34]D. E. Beck and V. Celli, Phys. Rev. Lett. **28**, 1124 (1972); Surf. Sci. **37**, 48 (1973).
[35]N. D. Lang and W. Kohn, Phys. Rev. B **3**, 1215 (1971).
[36]The numbers listed in Ref. 16 as coming from Ref. 33 are incorrect [D. E. Beck (private communication)].
[37]J. E. Inglesfield and E. Wikborg, Solid State Commun. **14**, 661 (1974).
[38]The infinite barrier asymptotes in Fig. 4 are more accurately determined since the kernel in (51) is then known analytically (Refs. 8 and 32).